Miscibility Enhancement Through Hydrogen Bonding Interaction of Biodegradable Poly(3-hydroxybutyrate) Blending with Poly(styrene-*co*-vinyl phenol) Copolymer

Shiao-Wei Kuo, Wei-Chen Liu

Department of Materials and Optoelectronic Science, Center for Nanoscience and Nanotechnology, National Sun Yat-Sen University, Kaohsiung 804, Taiwan

Received 4 May 2009; accepted 30 March 2010
DOI 10.1002/app.32528
Published online 21 July 2010 in Wiley Online Library (wileyonlinelibrary.com).

ABSTRACT: Differential scanning calorimetry, one- and two-dimensional Fourier transform infrared (FTIR), and solid state nuclear magnetic resonance (NMR) spectroscopy have been used to investigate the miscibility of and specific interactions between poly(styrene-*co*-vinyl phenol) (PSOH) and poly(3-hydroxybutyrate) (PHB) upon varying the vinyl phenol content of the PSOH copolymer. The FTIR and solid state NMR spectra revealed that the phenol units of PVPh interact with the carbonyl groups of PHB through intermolecular hydrogen bonding. A miscibility window exists when the vinyl phenol fraction in the copolymer is greater than 22 mol % in the PSOH/PHB blend system, as predicted using the Painter–Coleman association model. © 2010 Wiley Periodicals, Inc. J Appl Polym Sci 119: 300–310, 2011

Key words: Poly(3-hydroxybutyrate); hydrogen bonding; copolymer; miscibility

INTRODUCTION

Poly(3-hydroxybutyrate) (PHB) is a biodegradable and biocompatible crystalline polymer that can be produced in microorganisms that possess similar thermal and mechanical properties to isotactic polypropylene.[1,2] PHB is also the most abundant polyester found in bacteria and the most extensively studied one in the family of poly(hydroxyalkanotes) (PHA).[3,4] As a result, microbial PHB has been attracted much attention as an environment degradable resin to be used for a wide range of agricultural, marine, and medical applications.[5] However, the practical use of PHB for these applications has been limited by its brittleness and narrow processing window because of its high crystallinity and high melting temperature, respectively. Therefore, different approaches have been explored to improve the performance of PHB polymer materials, including copolymerization and blending.[6] Hydroxybutyrate/hydroxyvalerate copolymers are the most important copolymers of this family. Although they are also highly crystalline polymers, increasing the HV content in the copolymer reduce the melting temperature and crystallinity, making the polymer more processable. Compared with the copolymerization method, blending may be a much easier and faster way to achieve the desired properties. Many blends containing PHB have been studied, such as blends with poly(vinyl phenol),[7–9] poly(ethylene oxide),[10–12], cellulose derivates,[13,14]poly(vinyl acetate),[6] and poly (lactic acid).[15]

Although new materials based on PHB exhibiting tunable properties can be prepared through the blending of two or more polymers, unfortunately, most polymer blends are immiscible because of their high degrees of polymerization; as a result, the entropic term becomes vanishingly small and the miscibility becomes increasingly dependent on the contribution of the enthalpic term. To enhance the formation of a miscible one-phase system in polymer blends, it is necessary to ensure that favorable specific intermolecular interactions exist between two base components of the blend. Blending hydroxyl groups containing polymers, such as PVPh,[16–21] phenolic resin,[22–29] and phenoxy resin[30–32] with polymers containing hydrogen bonding acceptor units, we can obtain potentially miscible system. PVPh is an interesting monomer with ring-substituted styrene derivatives that has been reported to form miscible blends with several polymers containing accessible "proton-acceptor" or "proton-donor" groups, such as acrylate, ester, ether, pyridine, and hydroxyl groups through the formation of hydrogen bond interactions.[16–21] Iriondo and Xing et al. reported that the PHB can form miscible blend with PVPh through

Correspondence to: S.-W. Kuo (kuosw@faculty.nsysu.edu.tw).

Contract grant sponsor: National Science Council, Taiwan, Republic of China under; contract grant numbers: NSC 97-2221-E-110-013-MY3, NSC 97-2120-M-009-003.

TABLE I
Characteristics of the Poly(styrene-*co*-vinyl phenol) Samples

Copolymer	Phenol ratio (mol %)[a]	Abb. name	M_n[b]	M_w/M_n[b]	T_g (°C)	T_d[c](°C)
PS	0	PS	8000	1.21	90	371
PVPh3-*r*-PS97	2.8	PSOH3	21,000	2.02	96	370
PVPh5-*r*-PS95	4.6	PSOH5	22,000	2.03	101	370
PVPh22-*r*-PS78	21.5	PSOH22	24,000	2.05	104	368
PVPh36-*r*-PS64	36.0	PSOH36	17,400	2.05	118	365
PVPh55-*r*-PS45	55.2	PSOH55	23,200	2.10	154	359
PVPh78-*r*-PS22	77.8	PSOH78	24,400	2.34	162	353
PVPh	100	PVPh	20,000	1.07	175	352

[a] Obtained from ^{1}H NMR spectrum.
[b] Obtained through GPC analysis.
[c] 5 wt % loss decomposition temperature

hydrogen bonding based on the observation of a single-dependent glass transition temperature.[7,8] In addition, a depression of the melting temperature of PHB is observed through the addition of PVPh content.

The motivation of this study is to investigate the minimum vinylphenol content in poly(styrene-*co*-vinyl phenol) copolymer with PHB required to make a blend miscible. In previous studies of the roles of intermolecular association in miscibility enhancement, we found that the incorporation of a small number of hydrogen bond acceptors or donors into a polystyrene chain renders the modified polymer miscible.[25,33,34] The aims of this study were (1) to investigate blends of PHB and the PS-*co*-PVPh copolymer, (2) to use 1D and 2D Fourier transform infrared (FTIR) spectroscopy to provide evidence for specific intermolecular association, and (3) to use the Painter–Coleman association model (PCAM) to predict whether a miscibility window exists for PHB/PS-*co*-PVPh blends.[35,36]

EXPERIMENTAL

Materials

PHB (weight-average molecular weight: 293,000 g/mol) was obtained from Aldrich. Poly(styrene-*co*-vinyl phenol) copolymers were synthesized through copolymerization of styrene and 4-*tert*-butoxystyrene. The monomer reactivity ratios [r_1 (styrene) = 1.02; r_2 (4-*tert*-butoxystyrene) = 0.80] were determined using the methodology of Kelen and Tudos;[37,38] several copolymers containing various contents of 4-*tert*-butoxystyrene were obtained.[39] The solution copolymerization of styrene with 4-*tert*-butoxystyrene in benzene was performed at 70°C under an argon atmosphere within glass reaction flasks equipped with condensers. AIBN was employed as the initiator; the mixtures were stirred for ca. 24 h. To determine the reactivity ratios, samples of the copolymers were taken from the reaction flasks during the early stages of copolymerization, i.e., when the degrees of conversion were low (4–9%). The copolymers were purified through a process of repeated precipitation in methanol/water (3:7, v/v) from THF solutions. The synthesized poly(styrene-*co*-4-*tert*-butoxystyrene) (PS-*co*-P*t*BOS) was dissolved in dioxane at a concentration of 10% (w/v). The solution was then heated under reflux overnight in the presence of 37% HCl to remove the *tert*-butoxy groups. Before vacuum drying, the poly (styrene-*co*-vinyl phenol) (PS-*co*-PVPh or PSOH) was precipitated repeatedly from THF solution into methanol/water and then purified through Soxhlet extraction with water for 72 h to remove any residual HCl. The copolymers were characterized using nuclear magnetic resonance (NMR) and FTIR spectroscopy, differential scanning calorimetry (DSC), and gel permeation chromatography (GPC). Table I lists the monomer feed ratios and resultant copolymer compositions of the PSOH copolymers.

Blend preparation

Blends of PSOH/PHB were prepared through solution blending. DMF solutions containing 5 wt % of the polymer mixture were stirred for 6–8 h; the solvent was then left to evaporate slowly at room temperature for 24 h. The blend films were then dried at 50°C for 2 days.

Characterization

Molecular weights and molecular weight distributions were determined at 35°C through GPC using a Waters 510 HPLC equipped with a 410 differential refractometer, a UV detector, and three Ultrastyragel columns (100, 500, and 10^3 Å) connected in series; THF was the eluent; the flow rate was 0.6 mL/min. The molecular weight calibration curve was obtained using polystyrene standards. ^{1}H-NMR and ^{13}C-NMR spectra were obtained using an INOVA 500 instrument; acetone-d_6 was the solvent. The glass

transition temperatures (T_g) of the polymer blend films were determined through DSC using a TA Q-20 instrument. The scan rate was 20°C/min within the temperature range 30–200°C; the temperature was then held at 200°C for 3 min to ensure complete removal of residual solvent. The T_g measurements were performed in the DSC sample cell after the sample (5–10 mg) had been cooled rapidly to –50°C from the melt of the first scan. The glass transition temperature was defined at the midpoint of the heat capacity transition between the upper and lower points of deviation from the extrapolated liquid and glass lines. FTIR spectra of the polymer blend films were recorded using the conventional KBr disk method. A THF solution containing the blend was cast onto a KBr disk and dried under conditions similar to those used in the bulk preparation. The film used in this study was sufficiently thin to obey the Beer–Lambert law. FTIR spectra were recorded using a Bruker Tensor 27 FTIR spectrophotometer; 32 scans were collected at a spectral resolution 1 cm^{-1}. Because polymers containing OH groups are hygroscopic, pure nitrogen gas was used to purge the spectrometer's optical box to maintain the sample films' dryness. Generalized 2D correlation analysis was performed using the 2D Shige software developed by Shigeaki Morita (Kwansei-Gakuin University, Japan). In the 2D correlation maps, white-colored regions are defined as positive correlation intensities; shaded regions are defined as negative correlation intensities. High resolution solid state ^{13}C-NMR experiments were carried out at room temperature using a Bruker DSX-400 Spectrometer operating at resonance frequencies of 399.53 and 100.47 MHz for ^{1}H and ^{13}C, respectively. The ^{13}C CP/MAS spectra were measured with a 3.9 μs 90° pulse, with 3 s pulse delay time, acquisition time of 30 ms and 2048 scans were accumulated. All NMR spectra were taken at 300 K using broad band proton decoupling and a normal cross-polarization pulse sequence. A magic angle sample spinning (MAS) rate of 5.4 kHz was used to eliminate resonance broadening because of the anisotropy of chemical shift tensors.

RESULTS AND DISCUSSION

Analyses of PVPh/PHB blends

Thermal characterization of polymer blend is a DSC analysis is one of the most convenient methods available to determine the miscibility of polymer blends. Miscibility between any two polymers in the amorphous sate is detected by the presence of a single glass transition temperature. Moreover, the T_g of a blend has an important effect on the mobility of the blend, and hence, on the rate of crystallization at a specified crystallization temperature. As a result, it is important to understand the T_g behavior of PVPh/PHB blends. Figure 1 displays the DSC thermograms of PVPh/PHB blends of various compositions; each of the PVPh/PHB blends possesses a single glass transition temperature, strongly suggesting that they are fully miscible blends exhibiting a homogeneous amorphous phase. Cold crystallization was found in pure PHB and the blend containing a PVPh content up to 20 wt % in the heating scan of quenched samples. Over the years, a number of equations have been offered to predict the variation of the glass transition temperature of a miscible blend as a function of composition. The most popular equation is the Kwei equation:[40]

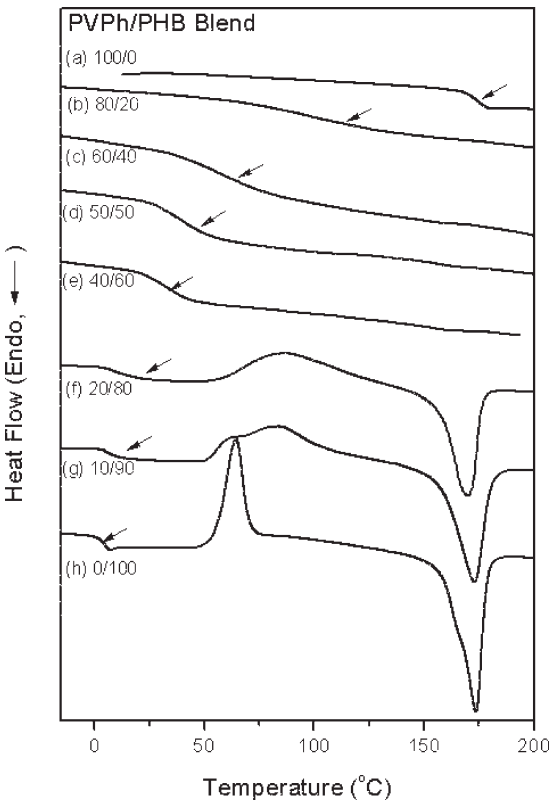

Figure 1 DSC thermograms of various PVPh/PHB blends.

$$T_g = \frac{W_1 T_{g1} + kW_2 T_{g2}}{W_1 + kW_2} + qW_1 W_2 \quad (1)$$

where W_1 and W_2 are the weight fractions of the components, T_{g1} and T_{g2} represent the corresponding glass transition temperatures, and k and q are fitting constants. Figure 2 present a plot of the dependence of the value of T_g on the composition of the miscible PVPh/PHB blends; values of k and q of 1 and –175 were obtained from the nonlinear least-squares "best fit." The parameter q corresponds to the strength of hydrogen bonding in the blend,

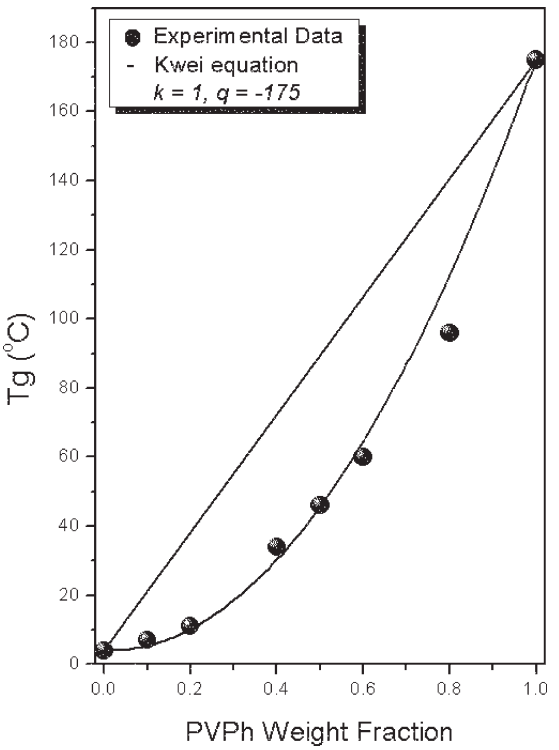

Figure 2 Plots of T_g with respect to composition, based on (■) experimental data and (—) the Kwei equation.

reflecting a balance between the breaking of self-associative and the forming of inter-associative hydrogen bonds. The negative value of q indicates that intermolecular hydrogen bonding was weaker than the intramolecular hydrogen bonding.

Figure 3 displays partial FTIR spectra (from 1630 to 1720 cm^{-1}) recorded at 25°C and 180°C for PVPh/PHB = 50/50. The C=O stretching frequency at 25°C appears split into at least three bands around 1742, 1724, and 1687 cm^{-1}, which are corresponding

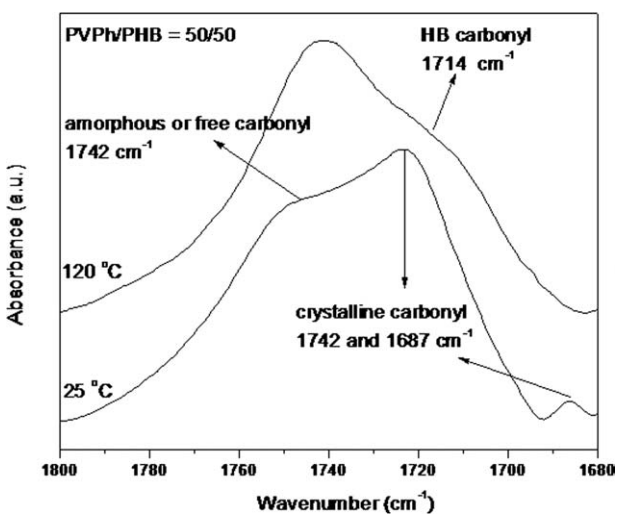

Figure 3 Partial FTIR spectra (1680–1800 cm^{-1}) of PVPh/PHB = 50/50 blend at 25°C and 180°C.

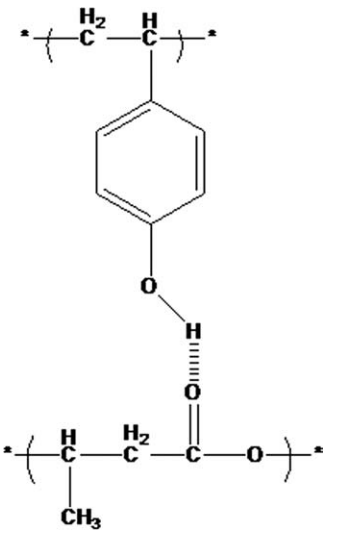

Scheme 1 The hydrogen bonding interaction scheme of PVPh/PHB blend

to amorphous C=O (1742 cm^{-1}) and crystalline C=O (1724 and 1687 cm^{-1}), respectively.[41–43] The spectrum at 180°C, registered during the heating process, the bands at crystalline C=O (1724 and 1687 cm^{-1}) disappear completely, indicating the PHB was totally melting. Meanwhile, a new absorption at 1714 cm^{-1} is attributed to the PHB carbonyl groups hydrogen bonded to the hydroxyl group of PVPh at 180°C as shown in Scheme 1. As a result, it was found that the quantitative fraction of hydrogen bonding was difficult to calculate because of four bands in carbonyl stretching at room temperature. For convenience, we turn our attention to the hydroxyl and carbonyl stretching region of the PVPh/PHB blends at 180°C for eliminating the crystallization effect.

Figure 4(b) shows the infrared spectra of the carbonyl stretching measured at 180°C ranging from 1690 to 1800 cm^{-1} for different compositions of PVPh/PHB blends. Clearly, the bands at 1742 and 1714 cm^{-1}, corresponding to free and the hydrogen-bonded C=O groups, respectively. The fraction of hydrogen-bonded C=O groups increased upon increasing the PVPh content. The bands were readily decomposed into two Gaussian peaks to determine the areas of the signals corresponding to the hydrogen-bonded (1714 cm^{-1}) and free (1742 cm^{-1}) C=O groups. The relative fractions of free and hydrogen-bonded C=O groups were calculated using an absorptivity coefficient of 1.5, i.e., the ratio of the intensity of the two bands.[15] Table II summarizes the spectral parameters for the C=O bands, and reveals that fraction of hydrogen-bonded C=O groups of PHB increased upon increasing the PVPh content.

Figure 4(a) displays partial FTIR spectra (OH stretching region; 2700–4000 cm^{-1}) of pure PVPh, pure PHB, and various PVPh/PHB blends. The pure

TABLE II
Parameters obtained after Curve Fitting Room-Temperature FTIR Spectra of PVPh/PHB Blends at 180 °C

	Free C=O			Hydrogen bonded C=O			
PVPh/PHB	ν, cm^{-1}	$W_{1/2}$, cm^{-1}	A_b (%)	ν, cm^{-1}	$W_{1/2}$, cm^{-1}	A_b (%)	f_b^a
80/20	1741	29	52.4	1714.3	30	47.6	37.7
60/40	1742	29	62.4	1714.3	31	37.6	28.7
50/50	1741	29	67.9	1714.2	30	32.1	23.8
40/60	1742	29	74.0	1714.3	31	26.0	18.9
20/80	1741	28	88.0	1714.2	30	12.0	8.3
0/100	1741	30	100.0	–	–	–	–

PVPh exhibits two bands in the OH stretching region: a very broad band centered at 3400 cm^{-1}, attributed to the wide distribution of the hydrogen-bonded OH groups, and a narrower shoulder band at 3525 cm^{-1}, representing free OH groups. The intensity of free OH absorption (3525 cm^{-1}) decreased gradually as the PHB content of the blend was increased from 20 to 80 wt %. The band for the hydrogen-bonded OH groups in the phenolic shifted to higher frequency (toward 3490 cm^{-1}) upon increasing the PHB content. This phenomenon resulted from a switch from OH···OH to OH···O=C hydrogen bonds. Therefore, it is reasonable to assign the band at 3490 cm^{-1} to the signal of the OH groups that were hydrogen-bonded to C=O groups. The frequency difference between the free and the hydrogen-bonded OH groups can be used to determine the average strength of the intermolecular interactions.[35] In this study, OH···O=C interassociation ($\Delta\nu$ = 35 cm^{-1}) was much weaker than the self-association of the OH groups of the phenolic ($\Delta\nu$ = 125 cm^{-1}), consistent with the negative value of q determined from the Kwei equation.

Inter-association equilibrium constant of PVPh/PHB Blend

Figure 5 provides a plot of the fraction of hydrogen-bonded C=O groups of PHB versus the PVPh weight fraction in the two-blend system. The PCAM[35] can be used to determine the equilibrium constants describing self-association and inter-association and other thermodynamic properties. The self-association equilibrium constants, K_2 and K_B, corresponding to the OH···OH interactions of phenolic, represent the formation of hydrogen-bonded "dimers" and "multimers," respectively. In this study, a suitable value for K_A of 25 for the PVPh/PHB blend was based on the experimental data and theoretical predictions. The calculation of the interassociation equilibrium constants using the least-squares method has been discussed previously.[23] The value of K_A, is smaller than that obtained for PVPh/amorphous PHB (K_A= 41).[44] In this study, we use semicrystalline PHB may decrease the interassociation equilibrium constant.[45] Table III lists all of the parameters required by the PCAM to estimate the thermodynamic properties of these polymer blends. Clearly, the interassociation equilibrium constant of PVPh/PHB is weaker than the self-association equilibrium constant of pure PVPh, which results in the negative value of q.

Two-dimensional correlation analysis of PVPh/PHB blends

White and shaded areas in 2D-IR correlation contour maps represent positive and negative cross-peaks, respectively. 2D-IR correlation spectra are characterized by two independent wavenumber axes and a correlation intensity axis. In general, two types of spectra, 2D synchronous and asynchronous, are obtained; the correlation intensities in the 2D synchronous and asynchronous maps reflect the relative degrees of in-phase and out-of-phase responses, respectively. The 2D synchronous spectra are symmetric with respect to the diagonal line in the correlation map. Auto peaks, which represent the degree of autocorrelation of perturbation-induced molecular vibrations, are located at the diagonal positions of a synchronous 2D spectrum; their values are always

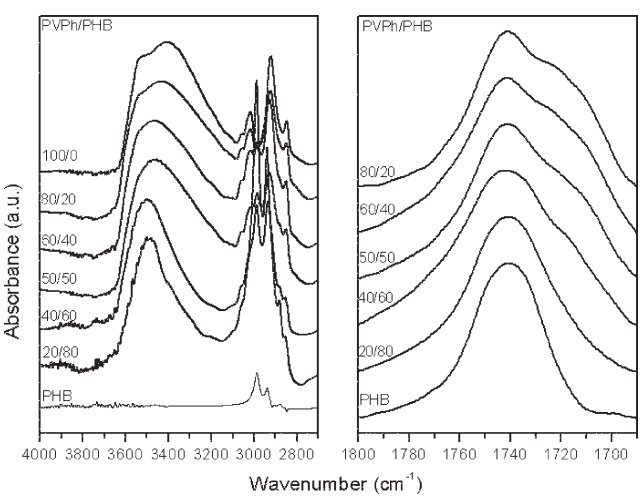

Figure 4 FTIR spectra of various PVPh/PHB blends at 180°C of (a) hydroxyl stretching and (b) carbonyl stretching.

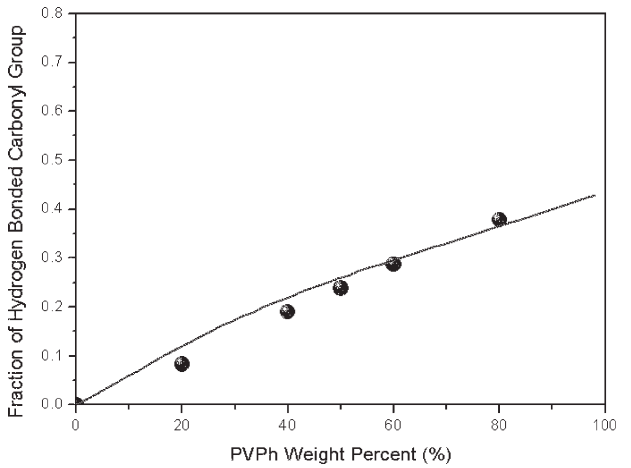

Figure 5 Plot of the fraction of the hydrogen-bonded C=O groups with respect to composition: (■) FTIR spectral data; (—) theoretical values for polymer blends calculated at 180°C.

positive. When an auto peak appears, the signal at that wavenumber would change greatly under environmental perturbation. Cross-peaks located at off-diagonal positions of a synchronous 2D spectrum (they may be positive or negative) represent the simultaneous or coincidental changes of the spectral intensity variations measured at v_1 and v_2. Positive cross-peaks result when the intensity variations of the two peaks at v_1 and v_2 occur in the same direction (i.e., both increase or both decrease) under the environmental perturbation; negative cross-peaks reveal that the intensities of the two peaks at v_1 and v_2 change in opposite directions (i.e., one increases while the other decreases) under perturbation.[46]

As in the case for a synchronous spectrum, the sign of an asynchronous cross peak can be either negative or positive, providing useful information on the sequential order of events observed by the spectroscopic technique along the external variable. The 2D asynchronous spectra are asymmetric with respect to the diagonal line in the correlation map. According to Noda's rule,[46] when $\Phi(v_1,v_2) > 0$, if $\psi(v_1,v_2)$ is positive (black colored area), band v_1 will vary before band v_2; if $\psi(v_1,v_2)$ is negative (white colored area), band v_2 will vary before band v_1. This rule is reversed, however, when $\Phi(v_1,v_2) < 0$. In summary, if the symbols of the cross-peak in the synchronous and asynchronous maps are the same (both positive or both negative), band v_1 will vary before band v_2; if the symbols of the cross-peak are different in the synchronous and asynchronous spectra (one positive and the other negative), band v_1 will vary after v_2 under the environmental perturbation.

Figure 6(a) presents the synchronous 2D correlation maps in the range 1500–1780 cm^{-1}. Absorption bands in this spectral range that are associated with PVPh appear at 1612, 1595, and 1510 cm^{-1}, corresponding to an in-plane C—C stretching frequency of a ring influenced by an OH group (phenyl-OH), the in-plane C—H stretching vibration of a ring influenced by an OH group, and another in-plane C—C stretching frequency of a ring influenced by an OH group (phenyl-OH), respectively; (cf. those of pure polystyrene at 1601, 1583, and 1493 cm^{-1}, respectively). Signals associated with PHB appear at 1742, 1and 1715 cm^{-1}, which are attributable to vibration of the free C=O groups, and hydrogen bonded C=O. Clear, two small positive cross-peaks existed between the signal at 1715 cm^{-1} and those at 1612 and 1510 cm^{-1}, implying the existence of hydrogen bonding between hydrogen bonded C=O groups of PHB (1715 $cm^{-1)}$ and phenol-OH groups (1612 and 1510 $cm^{-1)}$ of PVPh. The positive cross-peaks at 1715, 1612, and 1510 cm^{-1} all exhibit the same direction according to Noda's rule (both increase and both decrease under environment perturbation). On the contrary, the signal at 1742 cm^{-1} has two negative cross-peaks with those at 1612 and 1510 cm^{-1}, indicating that these latter two bands vary in the opposite direction to that at 1742 $cm^{-1.}$ Undoubtedly, these two functional hydroxyl groups should vary in opposite direction with the free carbonyl group.

Figure 6(b) displays the asynchronous 2D correlation maps in the range 1500–1780 $cm^{-1.}$ The auto-

TABLE III
Self-Association and Interassociation Equilibrium Constants and Thermodynamic Parameters for PS-*r*-PVPh/PVPK Blends at 25°C

				Equilibrium constant			Enthalpy (Kcal/mol)		
Polymer	V	M_w	δ	K_2	K_B	K_A	h_2	h_B	h_A
PVPh[a]	100.0	120.0	10.6	21.0	66.8	–	−5.6	−5.2	
PS[2]	93.9	104.1	9.48						
PHB[a]	69.8	86.0	9.61	–	–	25			−4.3

V: Molar Volume (ml/mol), M_w: Molecular Weight (g/mol), δ: Solubility Parameter $(cal/ml)^{1/2}$, K_2: Dimer self-association equilibrium constant, K_B: Multimer self-association equilibrium constant, K_A: Inter-association equilibrium constant, h_2: enthalpy of dimer self-association formation, h_B: enthalpy of multimer self-association formation and h_A: enthalpy of interassociation formation.

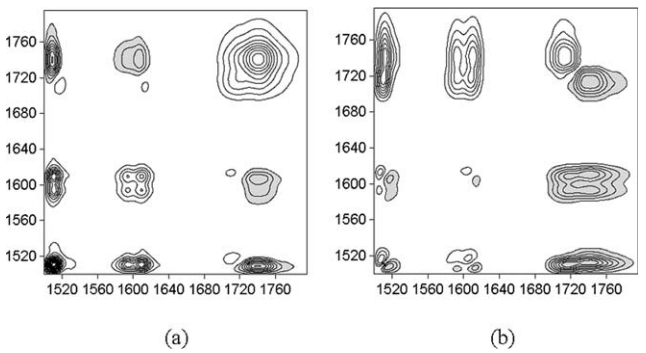

Figure 6 (a) Synchronous and (b) asynchronous 2D correlation maps for the region from 1500 to 1780 cm^{-1}.

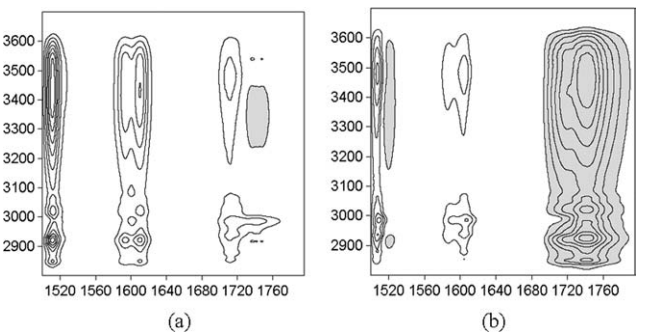

Figure 7 (a) Synchronous and (b) asynchronous 2D correlation maps for the regions from 1500 to 1780 cm^{-1} and from 2800 to 3700 cm^{-1}.

peak at 1742 cm^{-1} splits into the two separate bands for PHB located at ca. 1742 and 1715 cm^{-1}. This phenomenon suggests that there are two different C=O group sites in PHB. One, at the relatively lower wavenumber (1715 cm^{-1}), represents C=O groups involved in hydrogen bonding interactions with the OH groups of PVPh; the other, at higher wavenumber (1742 cm^{-1}), represents free C=O groups. This result is similar to the findings in the 1D FTIR spectra in Figure 4. Furthermore, the cross-peaks between the signal at 1742 cm^{-1} and those at 1612 and 1510 cm^{-1} in Figure 6(b) exhibit opposing intensity orders, indicating that these two bands result from different polymer chains, i.e., intermolecular hydrogen bonding. In addition, the cross-peaks among 1742 with 1715, 1742 with 1612 cm^{-1} and 1715 with 1612 cm^{-1} show opposite intensity order, indicating, implying that the peak of 1715 cm^{-1} alter before that of 1612 cm^{-1}, 1612 cm^{-1} alter before that of 1742 cm^{-1} during environment perturbation. In total, the 2D map reveals that the sequence of changing intensity of the three bands observed in the spectra is 1715 > 1612 >1742 cm^{-1}.

Figure 7 provides an analysis of the 1500–1780 and 2800–3700 cm^{-1} region, which represent the signals for OH and CH_3 stretching bands, to provide a macroscopic view of the interactions. The sign of the cross-peaks at (1742, 3400 cm^{-1}) and (1742, 2910 cm^{-1}) is negative in synchronous [Fig. 7(a)] map. Thus, we infer that the changes in intensity of these bands occur in the opposite direction, according to Noda's rule (one decreases, the other increases), meaning that the intensity of the signal for the free C=O group of PHB will decrease upon increasing the OH group content of PVPh and CH_3 group of PHB. Here, we pay attention to the interaction between the C=O and CH_3 groups of PHB. In previous study by Ozaki et al.,[41] the temperature-dependent wide-angle X-ray scattering (WAXS) study suggested that there are intermolecular interactions between the C=O and CH_3 groups in PHB, and the interactions decrease along the *a* axis of the crystal lattice of PHB with temperature. Subsequently, the existence and thermally induced changes of the C—H---O hydrogen bond between the C=O group and the CH_3 group were also verified by a temperature-dependent and 2D-IR spectroscopy study of PHB.[42] In addition, the signs of the cross-peaks at (1742, 3400 cm^{-1}), (1715, 3400 cm^{-1}), and (1742, 2900 cm^{-1}) are positive in asynchronous [Fig. 7(b)] maps. Taken together, the 2D analyses in Figures 6 and 7 suggest that the sequence of intensity increases is 2900 > 1714 > 3400 > 1612 > 1742 cm^{-1}. Thus, it appears that the hydrogen bonding between CH_3 and C=O of PHB initially deassociated and then phenyl-OH groups form hydrogen bonds with the C=O groups of PHB, consistent with the signal for the OH groups initially shifting to higher wavenumber upon increasing the PHB content (Fig. 4). Finally, the phenyl-OH groups of PVPh interact with the OH groups of PVPh and then interact with the free carbonyl of PHB.

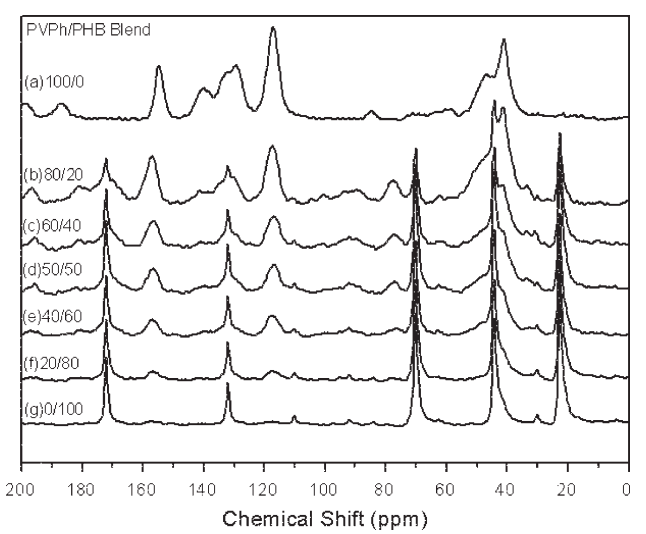

Figure 8 ^{13}C CP/MAS Solid State NMR of various PVPh/PHB blend at room temperature.

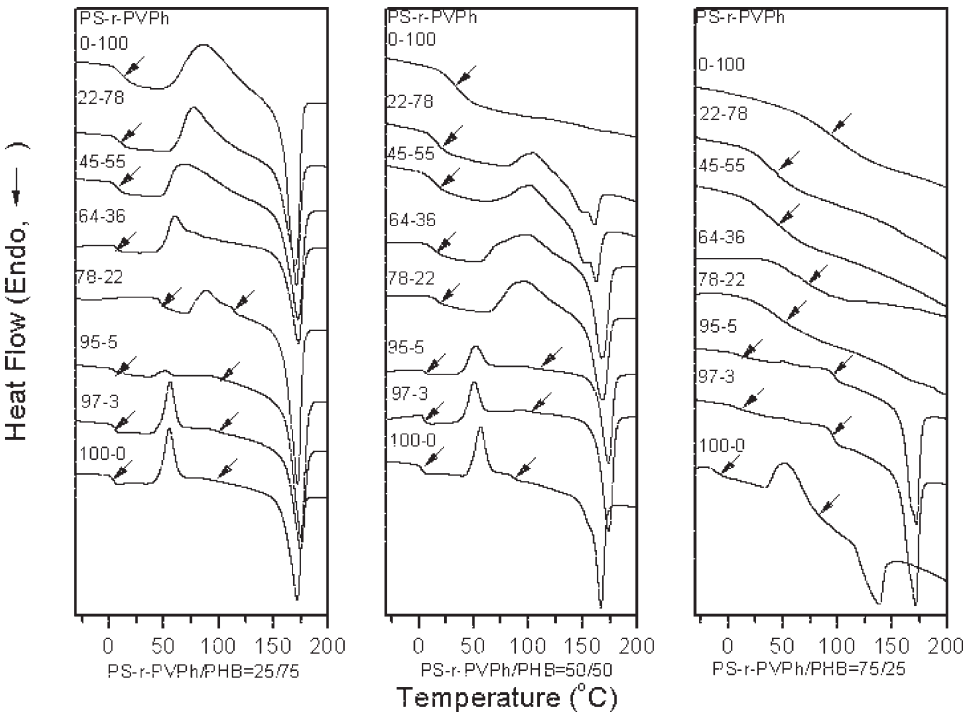

Figure 9 DSC curves of PSOH/PHB blends containing various amounts of PVPh.

Solid state NMR analyses

Solid-state NMR spectroscopy provides further quantitative information about specific interaction of polymer blend. The ^{13}C CP/MAS spectra of PVPh/PHB blends with various compositions at room temperature are shown in Figure 8, while Figure 8(a) shows the peak assignments of four major peaks. The hydroxyl substituted carbon in the phenolic ring (C—OH) has a resonance peak at 152.1 ppm, whereas the peaks at 115.8 and 129.4 ppm correspond to the ortho unsubstitituted carbon and the other carbons in the phenol ring, respectively.

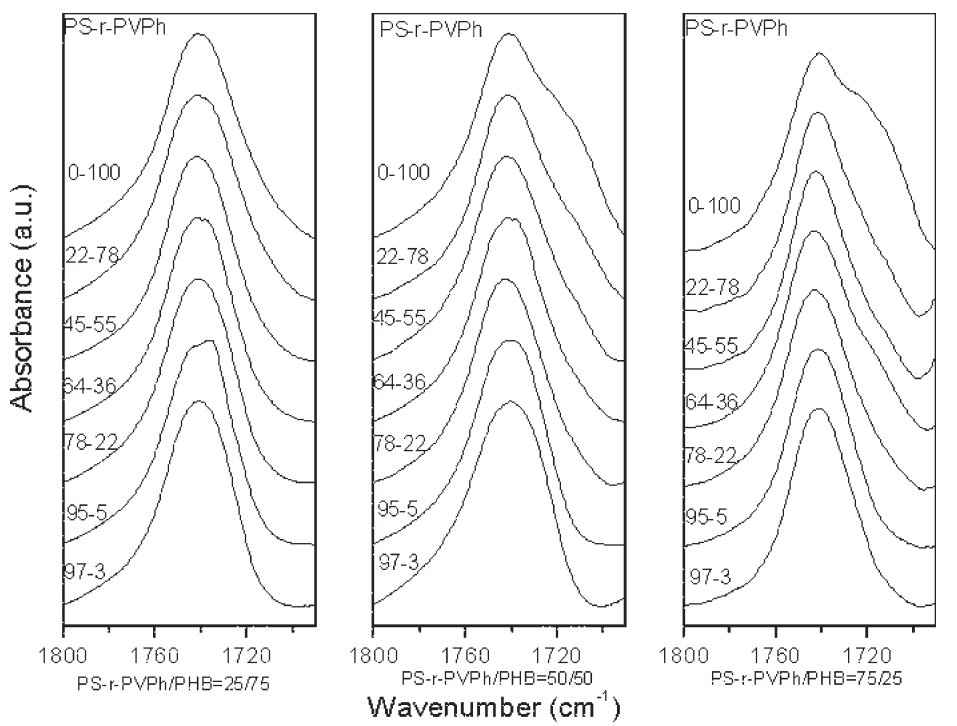

Figure 10 Partial FTIR spectra (1680–1800 cm^{-1}) of PSOH/PHB blends containing various amounts of PVPh.

TABLE IV
DSC Thermograms of PS-*co*-PVPh/PHB for Various PVPh Contents

PSOH/PHB = 25/75	T_g(°C)		T_m(°C)	T_c(°C)
PS	4	91	172	55
PSOH3	5	98	174	56
PSOH5	5	101	174	52
PSOH22	45	115	172	87
PSOH36	6		172	59
PSOH55	7		172	63
PSOH78	9		171	76
PVPh	11		170	84
PSOH/PHB =50/50				
PS	3	87	166	56
PSOH3	3	104	173	50
PSOH5	6	102	173	51
PSOH22	16		168	94
PSOH36	11		167	100
PSOH55	13		161	101
PSOH78	15		160	102
PVPh	34			
PSOH/PHB =75/25				
PS	−5	71	138	51
PSOH3	7	97	157	50
PSOH5	6	96	172	51
PSOH22	46			
PSOH36	68			
PSOH55	43			
PSOH78	32			
PVPh	93			

Meanwhile, the other resonance at 35 ppm corresponds to the methylene carbons. Figure 8(g) displays the spectrum of the PHB with four resonance peaks. All peak assignments of structures are assigned in Figure 8.

The line shape of the carbonyl carbon of PHB becomes broader with the increase of PVPh. It is well known that the existence of specific interaction in polymer blends will affect the chemical environment of the neighboring molecules and cause changes of magnetic shielding; therefore, the line shape becomes broader. In addition, chemical shift is observed for the hydroxyl-substituted carbon of PVPh, which shifts downfield with the increase of PHB amount. A downfield shift of 2.4 ppm is observed in the PVPh/PHB = 20/80 blend relative to the pure PVPh, indicating intermolecular hydrogen bonding between the hydroxyl group of PVPh and the carbonyl group of PHB. These results are consistent with the previous FTIR results (Figs. 3 and 4).

Analyses of PS-co-PVPh/PHB blend

The glass transition and melting behaviors of PHB blended with the various amounts of PS-*co*-PVPh were examined using DSC. Figure 9 displays typical results for selected PS-*co*-PVPh contents over a wide range of PVPh levels. Table IV summarizes whether one or two T_g values were noted for all PS-*co*-PVPh/PHB blends. Clearly, blends of PHB with PS-*co*-PVPh copolymers containing 22 mol % or more of PVPh exhibited a single glass transition, indicating complete miscibility within this window of PVPh contents. Figure 10 presents partial FTIR spectra (1680–1800 $cm^{-1)}$ measured at 120°C for PS-*co*-PVPh/PHB blends containing various amounts of PVPh in the PS-*co*-PVPh copolymers. Similar to the situation in the spectra in Figure 4, the C=O stretching bands of these blends are split into two signals, i.e., those for absorptions of free and hydrogen-bonded C=O groups at 1742 and 1715 cm^{-1}, respectively. Quantitative analyses of these C=O bands provides a direct measure of the degree of mixing in these polymer blends. The fraction of hydrogen-bonded C=O groups increased upon increasing of the PVPh content in the PS-*co*-PVPh copolymer. Therefore, the blend containing a higher PVPh content in the PS-*co*-PVPh copolymer forms a greater number of hydrogen bonds, thereby forming a one-phase system more preferably. The presence of a significant fraction of hydrogen bonds may result in a well-mixed system, but it does not necessarily imply the existence of a thermodynamically miscible blend. Fortunately, we can use the Painter–Coleman association model to calculate and define the miscibility window, taking advantage of the known molar volumes, molecular weights, solubility parameters, degrees of polymerization, and equilibrium constants (including self-association and inter-association) in Table III.

Miscibility window prediction

Painter and Coleman[36] suggested adding an additional term—accounting for the free energy of

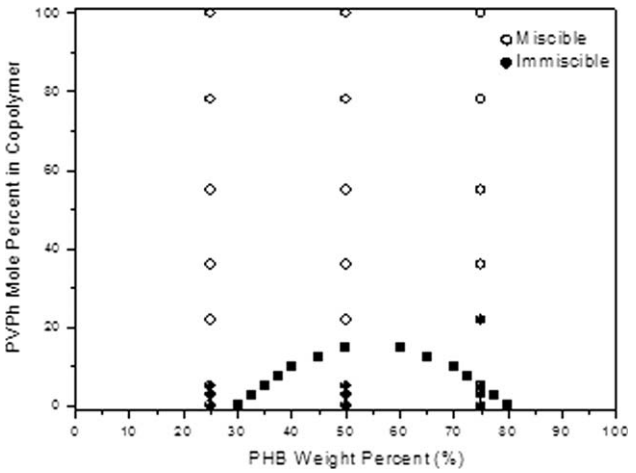

Figure 11 Theoretical miscibility windows for PVPh-*co*-PS/PHB blends obtained from the Painter–Coleman association model (▲) spinodal curve and experimental data: (●) two-phase system; (○) one-phase system.

hydrogen bond formation—to a simple Flory–Huggins expression for the free energy of mixing of two polymers:

$$\frac{\Delta G_N}{RT} = \frac{\Phi_1}{N_1}\ln\ \Phi_1 + \frac{\Phi_2}{N_2}\ln\ \Phi_2 + \Phi_1\Phi_2\chi_{12} + \frac{\Delta G_H}{RT} \quad (2)$$

where Φ and N are the volume fraction and the degree of polymerization, respectively, χ is the "physical" interaction parameter, and the subscripts 1 and 2 define the two blend components. ΔG_H is the free energy change contributed by hydrogen bonding between two components, which can be estimated from the FTIR spectra. According to the Painter–Coleman eq. (2), two major factors are responsible for this increase in the miscibility window. First, when the difference in the solubility parameters of the two polymer components of the blend decreases, the value of χ will decrease. Therefore, incorporation of PVPh (10.29 cal/cm^3) units into PS will increase the difference between the solubility parameters of PS (9.48 cal/cm^3) and PHB (9.6 cal/cm^3).[22] However, the relative number of inter-association upon increasing the PVPh content in the PS-*co*-PVPh copolymer, tending to enhance the favorable contribution from the $\Delta G_H/RT$ term in equation (2) and thereby result in a favorable trend for miscibility. Figure 11 displays the miscibility window for PS-*co*-PVPh/PHB blends at 200°C as predicted theoretically using the PCAM.[36] We choose this temperature to compare the theoretical and experimental data because it is above the glass transition temperature and because the DSC curves were obtained after quenching the sample from this temperature. Therefore, it is reasonable to calculate the miscibility window after quenching from 200°C, where equilibrium conditions are retained. The *x*-axis in Figure 11 represents the weight fraction of PS-*co*-PVPh in the blend; the *y*-axis represents the mole percentage of PVPh in the PS-*co*-PVPh copolymer. The plot suggests that PVPh will be completely miscible with PS-*co*-PVPh/PHB blends when the PVPh content is greater than 22 mol %. Thus, the model's predicted miscibility window at 180°C compares favorably with our experimental results based on DSC analyses.

CONCLUSIONS

The FTIR spectra revealed that the phenol units of PVPh interact strongly with the C=O groups of PHB through intermolecular hydrogen bonding. Incorporating vinyl phenol monomer into PS can enhance the miscibility of PS with PHB because the value of χ decreases and the degree of interassociation increases between the C=O groups of PHB and the OH groups of the PVPh units in the PS-*co*-PVPh copolymer. PHB was miscible with PS-*co*-PVPh copolymers having vinyl phenol contents greater than 22 mol %. The Painter–Coleman association model predicts the miscibility of this blend system well.

References

1. Sudesh, K.; Abe, H.; Doi, Y. Prog Polym Sci 2000, 25, 1503.
2. Ha, C.; Cho, W. Prog Polym Sci 2002, 27, 759.
3. Abe, H.; Doi, Y.; Aoki, H.; Akehata, T. Macromolecules 1998, 31, 1791.
4. Sato, H.; Nakamura, M.; Pademshoke, A.; Yamaguchi, H.; Terauchi, H.; Ekgasit, S.; Noda, I.; Ozaki, Y. Macromolecules 2004, 37, 3763.
5. King, P. P. J. Chem Tech Biotechnol 1982, 32, 2.
6. Huang, H.; Hu, Y.; Zhang, J.; Sato, H.; Zhang, H.; Noda, I.; Ozaki, Y. J Phys Chem B 2005, 109, 19175.
7. Iriondo, P.; Iruin, J. J.; Fernadez-Berrdi, M. J. Macromolecules 1996, 29, 5605.
8. Xing, P.; Dong, L.; An, Y.; Feng, Z.; Avella, M.; Martuscelli, E. Macromolecules 1997, 30, 2726.
9. Iriondo, P.; Iruin, J. J.; Fernandez-Berrdi, M. J. Macromolecules 1995, 36, 3235.
10. Chee, M. J. K.; Ismail, J.; Kummerlowe, C.; Kammer, H. W. Polymer 2002, 43, 1235.
11. Yang, H.; Li, Z. S.; Shin, T. K.; Choi, H. J.; Jhon, M. S. Polymer 2001, 42, 5737.
12. Zhang, L. L.; Deng, X. M.; Zhao, S. J.; Huang, Z. T. Polymer 1997, 38, 6001.
13. Scandola, M.; Ceccorulli, G.; Pizzoli, M. Macromolecules 1992, 25, 6441.
14. Ceccorulli, G.; Pizzoli, M.; Scanodola, M. Macromolecules 1993, 26, 6722.
15. Zhang, J.; Sato, H.; Furukawa, T.; Tsuji, H.; Noda, I.; Ozaki, Y. J. Phys Chem B 2006, 110, 24463.
16. Kuo, S. W.; Chang, F. C. Macromolecules 2001, 34, 5224.
17. Kuo, S. W.; Chang, F. C. J Phys Sci Polym Phys 2002, 40, 1661.
18. Lin, C. L.; Chen, W. C.; Liao, C. S.; Su, Y. C.; Huang, C. F.; Kuo, S. W.; Chang, F. C. Macromolecules 2005, 38, 6435.

19. Kuo, S. W.; Liu, W. P.; Chang, F. C. Macromol Chem Phys 2005, 206, 2307.
20. Lee, H. F.; Kuo, S. W.; Huang, C. F.; Lu, J. S.; Chan, S. C.; Chang, F. C. Macromolecules 2006, 39, 5458.
21. Chen, W. C.; Kuo, S. W.; Jeng, U. S.; Chang, F. C. Macromolecules 2008, 41, 1401.
22. Huang, M. W.; Kuo, S. W.; Wu, H. D.; Chang, F. C.; Fang, S. Y. Polymer 2002, 43, 2479.
23. Kuo, S. W.; Chang, F. C. Macromol Chem Phys 2001, 202, 3112.
24. Kuo, S. W.; Lin, C. L.; Chang, F. C. Polymer 2002, 43, 3943.
25. Kuo, S. W.; Chang, F. C. Polymer 2001, 42, 9843.
26. Kuo, S. W.; Chang, F. C. Macromol Chem Phys 2002, 203, 868.
27. Kuo, S. W.; Chan, S. C.; Chang, F. C. J Polym Sci Polym Phys 2004, 42, 117.
28. Huang, C. F.; Kuo, S. W.; Lin, H. C.; Chen, J. K.; Chen, Y. K.; Xu, H.; Chang, F. C. Polymer 2004, 45, 5913.
29. Huang, C. F.; Kuo, S. W.; Lin, F. J.; Huang, W. J.; Wang, C. F.; Chang, F. C. Macromolecules 2006, 39, 300.
30. Kuo, S. W.; Chan, S. C.; Chang, F. C. Macromolecules 2003, 36, 6653.
31. Kuo, S. W.; Lin, C. L.; Wu, H. D.; Chang, F. C. J Polym Res 2003, 10, 87.
32. Kuo, S. W.; Chan, S. C.; Wu, H. D.; Chang, F. C. Macromolecules 2005, 38, 4729.
33. Kuo, S. W.; Chang, F. C. Macromolecules 2001, 34, 7737.
34. Kuo, S. W. Polymer 2008, 49, 4420.
35. Coleman, M. M.; Graf, J. F.; Painter, P. C. Specific Interactions and the Miscibility of Polymer Blends; Technomic Publishing: Lancaster, PA, 1991.
36. Coleman, M. M.; Painter, P. C. Miscible Polymer Blend-Background and Guide for Calculations and Design; DEStech Publications: Lancaster, PA, 2006.
37. Kennedy, J. P.; Kelen, T.; Tudos, F. J Polym Sci: Polym Chem Ed 1975, 13, 2277.
38. Kelen, T.; Tudos, F. F. Macromol Sci Chem 1975, 9, 1.
39. Lin, H. C.; Wang, C. F.; Kuo, S. W.; Tung, P. H.; Lin, C. H.; Chang, F. C. J Phys Chem B 2007, 111, 3404.
40. Kwei, T. K. J Polym Sci Polym Lett Ed 1984, 22, 307.
41. Sato, H.; Murakami, R.; Padermshoke, A.; Hirose, F.; Senda, K.; Noda, I.; Ozaki, Y. Macromolecules 2004, 37, 7203.
42. Zhang, J.; Sato, H.; Noda, I.; Ozaki, Y. Macromolecules 2005, 38, 4274.
43. Furukawa, T.; Sato, H.; Murakami, R.; Zhang, J.; Duan, Y.; Noda, I.; Ochiai, S.; Ozaki, Y. Macromolecules 2005, 38, 6445.
44. Gonzalez, A.; Irusta, L.; Fernandez-Berridi, M. J.; Iriarte, M.; Iruin, J. J. Polymer 2004, 45, 1477.
45. Kuo, S. W.; Chang, F. C. Macromolecules 2001, 34, 4089.
46. Noda, I.; Ozaki, Y. Two-Dimensional Correlation Spectroscopy; Wiley: 2004.